Multidiagnostic analysis of ultrafast laser ablation of metals with pulse pair irradiation

S. Amoruso,[1,2,a] R. Bruzzese,[1,2] X. Wang,[2] G. O'Connell,[3] and J. G. Lunney[3]
[1]*Dipartimento di Scienze Fisiche, Università degli Studi di Napoli Federico II, Complesso Universitario di Monte S. Angelo, Via Cintia, I-80126 Napoli, Italy*
[2]*CNR-SPIN, Complesso Universitario di Monte S. Angelo, Via Cintia, I-80126 Napoli, Italy*
[3]*School of Physics, Trinity College–Dublin, Dublin 2, Ireland*

(Received 31 August 2010; accepted 16 October 2010; published online 3 December 2010)

Copper targets are irradiated in the ablation regime by pairs of equal, time-delayed collinear laser pulses separated on a timescale going from ≈2 ps to ≈2 ns. The ablation plume is characterized by ion probe diagnostic, fast imaging, and temporally and spatially resolved optical emission spectroscopy. The variation in the ablation efficiency with the delay between the pulses is analyzed by measuring the ablation crater profile with a contact profilometer. The second laser pulse modifies the characteristics of the plasma plume produced by the first pulse and the ablation efficiency. The different mechanisms involved in double pulse ultrafast laser ablation are identified and discussed. The experimental findings are interpreted in the frame of a simple model of the interaction of the second pulse with the nascent ablation plume produced by the first pulse. This model yields consistent and quantitative agreement with the experimental findings predicting the observed experimental trends of the ablation depth reduction and ion yield increase with the delay between the pulses, as well as the characteristic timescale of the observed changes. The possibility of controlling the characteristics of the plumes produced during ultrafast laser ablation via an efficient coupling of the energy of the second pulse to the various ablation components produced by the first pulse is of particular interest in ultrafast pulsed laser deposition and microprobe analyses of materials. © *2010 American Institute of Physics*. [doi:10.1063/1.3516491]

I. INTRODUCTION

Ultrafast laser ablation (ULA) is attracting a lot of attention as a unique material processing technique that covers several contiguous application areas: e.g., nanoparticle (NP) generation, film growth, material processing, and laser-induced breakdown spectroscopy (LIBS). This has stimulated interest in both deeper physical understanding of the ULA process and strategies aiming to modify or control the properties of the ablated species and ablation craters.[1–5]

The ULA process has been extensively studied both theoretically and experimentally.[6–13] In ULA of metals, the pulse energy is absorbed by the conduction band electrons with a rapid increase in their temperature and pressure. Then, for times t lower than the electron-lattice relaxation time τ_{el} (typically ≈10 ps for elemental metals), the energy is progressively transferred to the lattice which increases its temperature and melts. At time t of the order of τ_{el}, a sharp pressure profile is generated in a narrow zone near the target surface. This leads to the generation of an intensive compressive wave that moves into the irradiated material, and of an associated rarefaction wave whereby material flows away from the target surface. The target decomposition is generally examined by following the thermodynamic trajectories of different layers in the phase diagram of the target material.[6–9] The surface layers of the target reach temperatures well above the critical temperature of the material and then relax directly through a rapid expansion into an atomic plume. The deeper layers, instead, relax following thermodynamic trajectories which pass near or below the critical point of the material, finally, decomposing into a plume of NPs through mechanical fragmentation and phase explosion. These last decomposition mechanisms describe the major part of the ablated material.[2,6,7,14]

This scenario is coherent with the experimental findings of a recent study on the early stages (≤30 ns) of the ULA of an Al metallic target.[15] By using ultrafast time-resolved x-ray absorption spectroscopy (time resolution=30 ps), this study observed that material ejection from the target surface starts within the first 30 ps and lasts for few tens of ns. The different ablation species (ions, atoms and NPs) are ejected sequentially from the surface, forming a structured nascent plume with the faster atomic species followed by a mixed phase containing hot-liquid NPs which are moving more slowly. The velocities of these populations are consistent with those of the atomic and NP plumes predicted by molecular dynamics simulations and measured at few mm from the target surface for ULA of an Al target in vacuum.[16]

The above comments indicate that the use of temporally shaped pulses or irradiation with a pair of equal laser pulses [double pulse (DP)] with controlled temporal separation may offer interesting routes to modify the properties of the ULA process thanks to the effects brought about by the interactions with a modified target surface or with the different components of the nascent ablation material. These two approaches are complementary. Shaped pulses within a temporal window of few tens of picoseconds allow variation in the

[a]Author to whom correspondence should be addressed. Electronic mail: amoruso@na.infn.it.

excitation sequence of the target on the timescale of the electron-phonon relaxation time. DP irradiation facilitates tuning of the properties of the ablation plume, depending on the temporal delay of the second pulse with respect to the ablation pulse. Some of these studies have shown that it is possible to: (i) modify the composition and shape of the laser-produced plasma;[1–4] (ii) control the size distribution of silicon NPs or the ionic/neutral emission ratio of a metallic Al plasma;[17,18] (iii) change the characteristics of the ablation craters;[1,5] and (iv) improve signal intensity and reproducibility in LIBS.[19] Thus, an effort is underway to get deeper understanding of the different physical mechanisms involved in these processes with the aim of improving the control of laser-induced ablation and plasma formation processes of interest in methods like laser microprocessing, LIBS, pulsed laser deposition, and so forth.

DP ULA experiments for different metals (e.g., Ag, Al, Au, Cu, and Ni) have also shown a surprising reduction in the ablation efficiency with the increase in the delay between the laser pulses.[1,2,20,21] This effect was observed both under vacuum and in air, at fluence levels in the range from few to ten times the ablation threshold. When the delay between the pulses, Δt is much shorter than τ_{el}, the ablation efficiency is almost independent of the delay. For $\Delta t \geq \tau_{el}$, the ablation efficiency decreases monotonically, finally, reaching a plateau regime for $\Delta t \approx 100$ ps ($\Delta t \gg \tau_{el}$), where it can reach values even smaller that that obtained by a single pulse (SP) only. Recently, the suppression of the ablation efficiency has been analyzed by detailed hydrodynamic modeling for the case of DP ULA of a copper target irradiated by 100 fs pulses at 800 nm, and related to the formation of a second shock wave induced by the interaction of the second laser pulse with the expanding target material which suppress the rarefaction wave created by the first pulse, thus lowering the ablation yield.[22] This study also showed that for delay $\Delta t \approx 50$ ps the second pulse can be efficiently absorbed (an absorption coefficient of ≈35% was estimated) by a front layer of the nascent ablation material located at a distance of ≈100 nm from the original target surface, in agreement with previous experimental considerations.[1,20] Therefore, it is possible to selectively couple more or less energy to one of the various ablated components, which can be of interest in various fields.

The investigations carried out so far have enabled some understanding of DP ULA, although most of the experiments examine specific features of the process, such as ablated depth, ablation plume dynamics, or plume emission enhancement, sometimes on a reduced range of delays between the pulses. It seems that an experiment that examines the simultaneous behavior of several features may be useful. In a recent letter,[23] we reported how DP irradiation of Cu, with delays Δt from 2 ps to 2 ns, leads to interesting modifications of the plume properties arising from the coupling of the second pulse with the nascent ablation material. Here, we aim to extend our previous analysis to further illustrate and discuss the role of the delay between the two pulses on the various characteristics of the ULA process. The DP ablation plume was studied by exploiting time- and space-resolved optical emission spectroscopy, fast imaging, and ion probe techniques, while the ablation efficiency was characterized by analyzing the crater depth profile with a contact profilometer.

II. EXPERIMENTAL METHODS

DP ULA experiments were carried out with a laser source emitting ≈250 fs pulses at 527 nm. These laser pulses were obtained by the second harmonic-generation and pulse compression of the fundamental output (i.e., 1055 nm, ≈0.9 ps) of a Nd:glass laser system. The temporal profile of the laser pulse was monitored by a single shot background free autocorrelation technique. The emitted energy per pulse was of the order of ≈1 mJ at 527 nm at a typical repetition rate of 33 Hz. The average fluence F was obtained as E/S, where E is the incident laser energy and S is the spot area estimated by measurement of the laser impact region as a function of the laser pulse energy.[24] During the experiments the repetition rate can be reduced by means of a mechanical shutter. A Michelson interferometer was used to split the beam in two different arms with equal energy, one of them equipped with a micrometer resolution motorized translation stage which introduces a controlled time delay, Δt, between the laser pulses within the range 0–2000 ps. Interference fringes were used to determine the condition $\Delta t = 0$. The two collinear laser pulses from the interferometer were focused on a copper target (99.9%) at an incidence angle of 45°, in high vacuum (10^{-7} mbar). The target was mounted on a rotating holder to avoid local drilling.

The ion plasma produced during the DP ULA process was monitored by using a negatively biased planar Langmuir probe.[25] The probe was oriented to face the target spot and located at a distance of 38 mm from the target along the normal of the target surface. The probe collecting area was a 2.5×5 mm^2 square copper plate, insulated on the rear side.

The plasma plume optical emission was imaged on the entrance slit of an imaging spectrograph equipped with a 300 grooves/mm grating coupled to an intensified-charge-coupled-device (ICCD). Two-dimensional (2D) single shot images of the plume were registered by operating the grating in reflection with the entrance slit fully open. Spectrally resolved, one-dimensional (1D) images of the plume emission, in the range 370–630 nm, were obtained by orienting the entrance slit of the spectrograph along the plume expansion axis. The spectrally resolved images were acquired by accumulation over 20 laser shots, to compensate the lower signal level and to reduce the noise. The ICCD was equipped with a 1024×1024 array and operated in time-gated detection mode. To reduce the noise, a $2\times$ binning was operated during image acquisition. ICCD gain and gate width were adjusted in order to achieve both a good accuracy of the plume propagation, and a reasonable signal-to-noise ratio of the plume images.

The ablation efficiency at some fixed delays between the pulses was found by irradiation of a stationary target with a fixed number of pulses ($N = 3300$), and measuring the ablation crater depth profile with a contact profilometer.

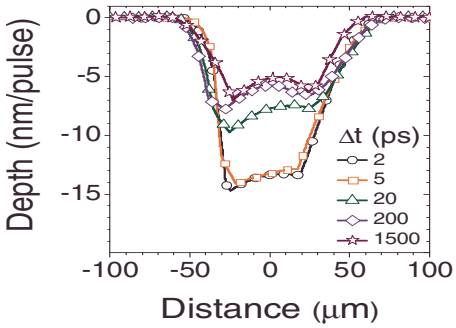

FIG. 1. (Color online) Typical depth profiles for copper ablation using DPs with various delays. The depth per pulse was obtained by dividing the measured depth by the number of pulses N.

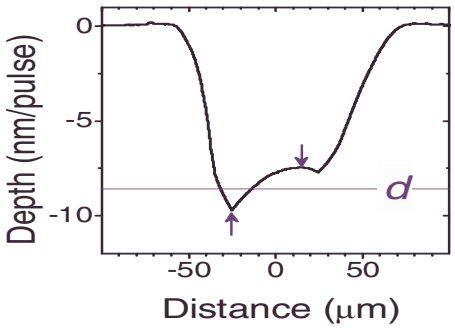

FIG. 2. (Color online) Crater depth profile showing the maximum and minimum depths of the crater bottom (arrows) from which d was estimated as an average.

III. EXPERIMENTAL RESULTS AND ANALYSIS

Prior to the DP experiment we measured the fluence threshold F_{th} for ablation of copper with a SP in our experimental conditions, estimating a value of $F_{th} \approx 0.15$ J/cm^2. The data presented below were obtained carrying out DP ULA experiments at a laser fluence of each pulse $F \approx 0.6$ J/cm^2, which corresponds to ≈ 4 times the ablation threshold of copper.

In the following we will illustrate the effects of the delay Δt on various characteristics of the DP ULA process. First, Sec. III A we will discuss the variation in the ablation efficiency with Δt for our experimental conditions. Then, we will address the effects of DP irradiation on the characteristics of the atomic and NP ablation plumes. In particular, the modifications of the DP irradiation on the ion features will be presented in Sec. III B, while in Sec. III C the atomic and NP plumes will be characterized by optical time-gated imaging and time- and space-resolved emission spectroscopy.

A. Ablation efficiency

In order to analyze the ablation efficiency, a stationary target was irradiated with a fixed number of pulses N at some selected delays Δt, and the depth profile along the minor radius of the elliptical crater produced on the target was measured. Some typical crater depth profiles are presented in Fig. 1. In all the cases the aspect ratio of the crater (i.e., the depth to diameter ratio) was below 1, thus minimizing any effect of deep-hole confinement on the estimate of the ablation rate per pulse. It has been shown earlier that in this condition the crater depth varies approximately linearly with the number of laser pulses,[26] therefore, the dependence of the ablation rate on the delay Δt was obtained by estimating the ablation depth per pulse d. As illustrated in Fig. 2, for each profile d was estimated by considering the average value between the maximum and minimum depths (arrows) of the crater bottom, and their difference was regarded as error bar. It is also worth noting that a very good consistency between the ablation depth and the crater volume was observed earlier in our experimental conditions,[1] therefore, we consider the ablation depth as a reliable measure of the ablation efficiency.

The variation in the maximum ablation depth with Δt is reported in Fig. 3; the dashed line shows the maximum ablation depth for SP irradiation. From Figs. 1 and 3 it is evident a clear dependence of the ablation efficiency on Δt. For short delay ($\Delta t \leq 5$ ps), d is of the order of 15 nm. As Δt is increased the ablation depth progressively decreases, approximately leveling off at a value of about 6 nm for $\Delta t \geq 100$ ps. A suppression of the ablation efficiency similar to that observed here was reported earlier for various elemental metallic targets (copper, aluminum, nickel, gold, and silver, e.g.)[1–3,21,22] thus indicating the existence of a common physical effect. In Fig. 2, the variation in the ablation depth d with the delay Δt is compared to an exponential function

$$d(\Delta t) = d_0 - \Delta d(1 - e^{-\Delta t/\tau_c}), \quad (1)$$

where $d_0 \approx 15$ nm corresponds to the ablation depth at zero delay, i.e., for a SP of twice the energy, $\Delta d \approx 9$ nm is the total depth variation and $\tau_c \approx 20$ ps is a characteristic time constant of the process. Time constants for the ablation depth reduction $\tau_c \approx 12$ ps for copper and $\tau_c \approx 30$ ps for gold were reported by Noel and Hermann during DP ULA with Ti:sapphire pulses at a fluence of 2 J/cm^2 per each pulse.[2] This was related to a change in the electron heat conductivity induced by the progressive increase in the lattice temperature occurring for delays larger than the electron-lattice thermalization time. Recently, Roberts *et al.*[21] studying DP ULA of silver foils observed that the time lag from the short delay region ($\Delta t < \tau_{el}$) to the plateau at large delay critically depends on the laser pulse fluence, decreasing from ≈ 100 ps at a fluence level of about 1 J/cm^2 to few picoseconds at ≈ 10 J/cm^2. This experimental observation might suggest that this characteristic time is not only related to the properties of the target but also to other effects such as energy

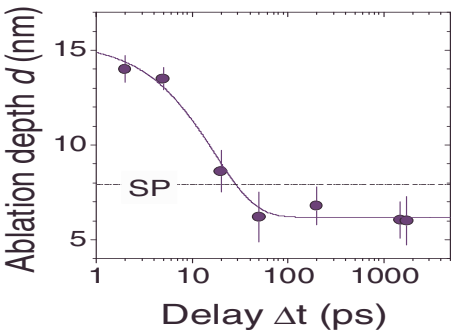

FIG. 3. (Color online) Maximum ablation depth d as a function of delay Δt between pulses. The solid curve is a fit to Eq. (1). The dashed line indicates the maximum ablation depth for SP irradiation.

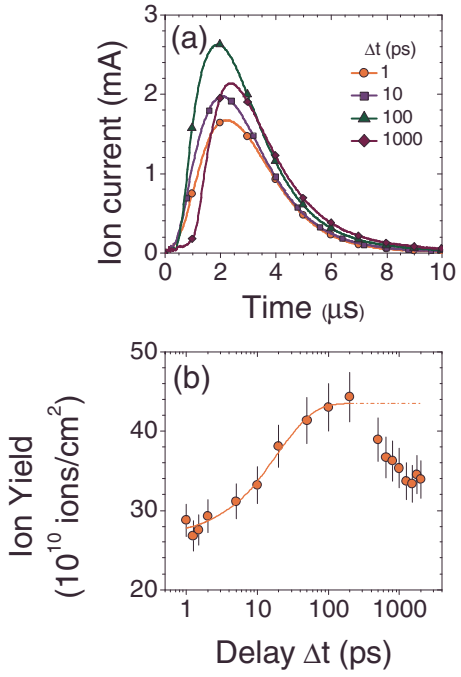

FIG. 4. (Color online) (a) Ion TOF signals for different delays between the two laser pulses. (b) Ion yield as a function of the delay between the pulses. The solid line is a fit to Eq. (2).

absorption in the nascent laser-produced plasma, as invoked in Refs. 1 and 20. Therefore, the interpretation of these experimental findings can benefit from the analysis of other features of the DP ULA process, as for instance the atomic and NP plume characteristics, which will be discussed hereafter.

B. Ion probe results

The influence of a second delayed pulse on the properties of the ion plasma produced during the DP ULA process was investigated by recording ion time-of-flight (TOF) signals, for different delays Δt, with a Langmuir probe. Figure 4(a) reports some characteristic ion profiles for various values of Δt. Both amplitude and TOF at the peak vary with the delay. In particular, as Δt increases from 1 ps to a few hundred picoseconds we observe a gradual rise of the signal amplitude which peaks at shorter TOF, thus indicating an increase in the ion yield and velocity. Conversely, at longer delays [see e.g., the profile at $\Delta t = 1000$ ps in Fig. 4(a)] the peak of the ion TOF profiles is gradually delayed while its amplitude progressively decreases. This behavior points to the existence of different interaction regimes as Δt varies in a temporal window of several hundred picoseconds.

The variation in the collected ion yield was obtained by integration of the ion profiles of Fig. 4(a). This is plotted in Fig. 4(b), which includes additional data points corresponding to delays not shown in Fig. 4(a). At $\Delta t \approx 1-2$ ps the DP ion yield is almost constant, it progressively increases reaching a maximum at $\Delta t \approx 200$ ps, and then decreases for longer delays.

In Fig. 4(b), the growth of the ion yield Y for 1 ps $< \Delta t < 200$ ps is well described by an exponential function[23]

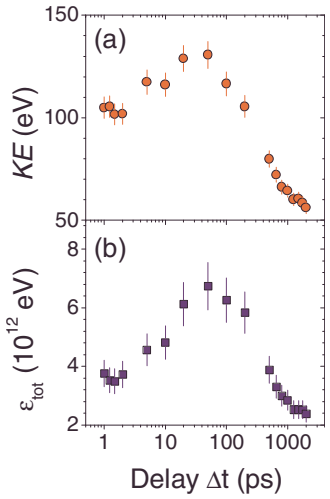

FIG. 5. (Color online) (a) Average kinetic energy KE of the ions as a function of the delay Δt between the pulses. (b) Total energy of the ion flux ε_{tot} as a function of the delay Δt between pulses.

$$Y(\Delta t) = Y_0 + \Delta Y(1 - e^{-\Delta t/\tau_c}), \tag{2}$$

where $Y_0 \approx 27 \times 10^{10}$ ions/cm^2 corresponds to the ion yield at zero delay, i.e., for a SP of twice the energy, $\Delta Y \approx 16.5 \times 10^{10}$ ions/cm^2 is the total variation in the ion yield, and $\tau_c \approx 20$ ps is a characteristic time constant of the process of ion increase induced by the DP irradiation. The fact that the exponential dependences of both the ion yield in Fig. 4 and the ablation depth in Fig. 3 are characterized by a very similar time constant $\tau_c \approx 20$ ps, supports the idea that the observed changes are related to the same physical mechanisms for 1 ps $< \Delta t < 200$ ps. At longer delays ($\Delta t > 200$ ps), instead, the ion yield drops down while the ablation efficiency seems to remain almost constant, thus indicating a progressive transition to another regime of the DP ULA process.

From the TOF signals in Fig. 4(a), the average ion kinetic energy (KE) was calculated and plotted in Fig. 5(a). For DP at $\Delta t \approx 1-2$ ps KE ≈ 100 eV, then it increases as the delay is increased, such that at $\Delta t = 50$ ps it is ≈ 130 eV. By further increase in the delay, KE decreases reaching values of $\approx 50-60$ eV which is even smaller than that observed at very short delays. From Figs. 4(b) and 5(a), we observe that the maximum of the ion yield and average energy is reached at two different delays, namely, ≈ 200 ps and ≈ 50 ps. Therefore, we analyzed the dependence on Δt of the total energy of the ion flux collected by the probe $\varepsilon_{tot}(\Delta t) = Y(\Delta t) \times \mathrm{KE}(\Delta t) \times S_p$, where S_p is the ion probe area. This is shown in Fig. 5(b). ε_{tot} shows a strong dependence on Δt: while there is little change for short delays ($\Delta t \approx 1-2$ ps), an increase in almost a factor of 2 is observed from short delay to $\Delta t \approx 50$ ps, where it reaches a maximum. For still longer delays ($\Delta t > 50$ ps), ε_{tot} gradually reduces reaching values even lower that the one observed at the shortest delays of 1–2 ps when $\Delta t \geq 650$ ps as a consequence of the combined reduction in the average energy of the ions KE and of its yield Y. The significant reduction in the average kinetic energy at long delays seems to be more related to the presence of ions with lower kinetic energy than to a decrease in the ion yield [see Figs. 4(b) and 5(a)]. To clarify this aspect, Fig.

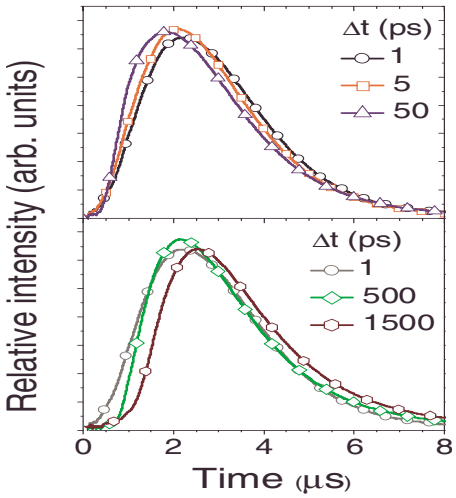

FIG. 6. (Color online) Examples of ion TOF profiles normalized to their corresponding area (relative intensity) at some delays showing the variation in the relative contribution of fast (small TOF, upper panel) and slow (large TOF, lower panel) ions to the TOF profile. In the lower panel the TOF profile at $\Delta t=1$ ps is shown in gray to facilitate the comparison.

6 shows some typical ion profiles from Fig. 4(a) normalized to the same area, from which the variation in the fast (small TOF) and slow (large TOF) ion contributions can be appreciated. Tacking $\Delta t=1$ ps as a reference TOF signal, in Fig. 6 one can notice: (i) an increase in the faster component with increasing delay up to ≈50 ps and (ii) a progressive reduction in the fast ions with a simultaneous increase in slow ions for long delays (e.g., $\Delta t=500$ ps and 1500 ps).

C. Optical imaging and spectroscopy

The effects of the second delayed pulse on the properties of the atomic and NP plumes produced during the DP ULA process was investigated by recording 2D single shot images of the plumes emission at various delays Δt. Figure 7(a) shows 2D maps of the atomic plume emission registered 200 ns after the ablating laser pulse. The region of high intensity clearly visible at 2 and 20 ps close to the target surface is the NP plume which has not yet fully expanded. The 2D maps of the NP plume emission after its expansion are shown in Fig. 7(b) which reports images registered ≈10 μs after the ablating laser pulse. Figure 7(a) indicates a progressive increase in the atomic plume emission intensity with the delay Δt, which is accompanied by a shortening of the plume extension along the direction z normal to the target surface. Moreover, the region of maximum intensity of the atomic plume moves toward the target surface as Δt increases. In Fig. 7(a), one can also observe that a distinct spatial separation between the atomic and NP plumes is present at short delays ($\Delta t=2$ and 20 ps). This separation gradually reduces as Δt increases, the two ablation components (atoms and NPs) becoming nearly connected for larger values of Δt. A strong effect of the delay Δt on the NP plume characteristics is evidenced in Fig. 7(b): both the NP plume emission intensity and spatial extension along the z-axis are significantly reduced as the delay Δt increases.

Figure 8 shows 1D spectrally resolved images of the atomic plume emission corresponding to the images of Fig.

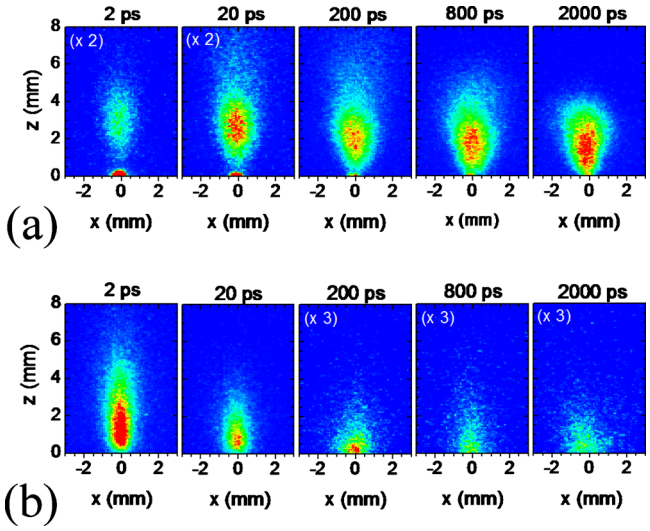

FIG. 7. (Color online) (a) Snapshots of the atomic plume emission at different delays Δt, acquired 200 ns after the ablating laser pulse with a gate width of 50 ns. (b) Snapshots of the NP plume emission at different delays Δt, acquired ≈10 μs after the ablating laser pulse with a gate width of 5 μs. The delay Δt is reported on the top of each image. The number in parenthesis in the top-left corner of the image indicates that the intensity has been multiplied by that factor. $z=0$ marks the position of the target surface. The intensity is plotted in linear scale.

7(a). The intensity is displayed on a logarithmic scale to compensate for the very different emission signal of the ablated species. In particular, in Fig. 8 we can identify:[27] (i) an intense signal at ≈490 nm located at the atomic plume front, which corresponds to the characteristic emission of excited ions (Cu^+) resulting from the overlap of different Cu^+ strong

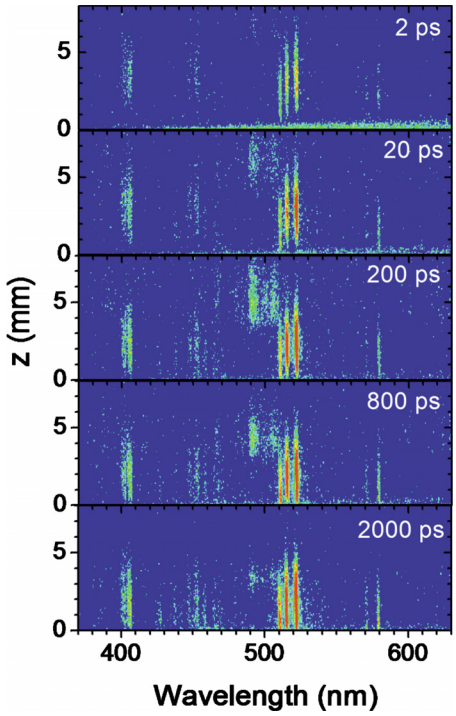

FIG. 8. (Color online) 1D spectrally resolved images of the atomic plume emission at different delays Δt, acquired 200 ns after the ablating laser pulse with a gate width of 50 ns. The delay Δt is reported in the top-right corner of each image. $z=0$ marks the position of the target surface. The intensity is plotted in logarithmic scale.

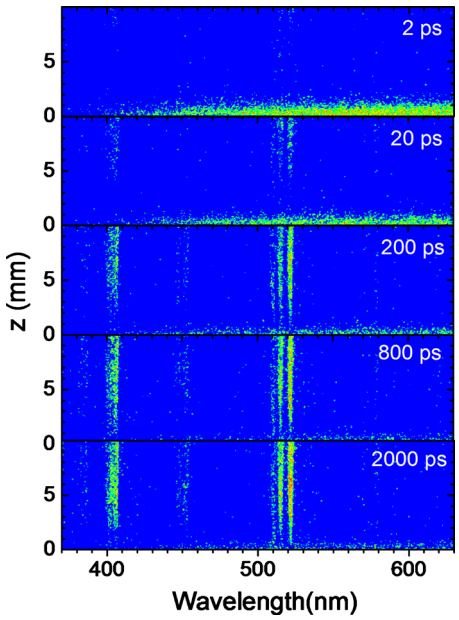

FIG. 9. (Color online) 1D spectrally resolved images of the atomic plume emission at different delays Δt, acquired 2 μs after the ablating laser pulse with a gate width of 1 μs. The delay Δt is reported in the top-right corner of each image. $z=0$ marks the position of the target surface. The intensity is plotted in logarithmic scale. The intensity scale is two times that used in Fig. 7.

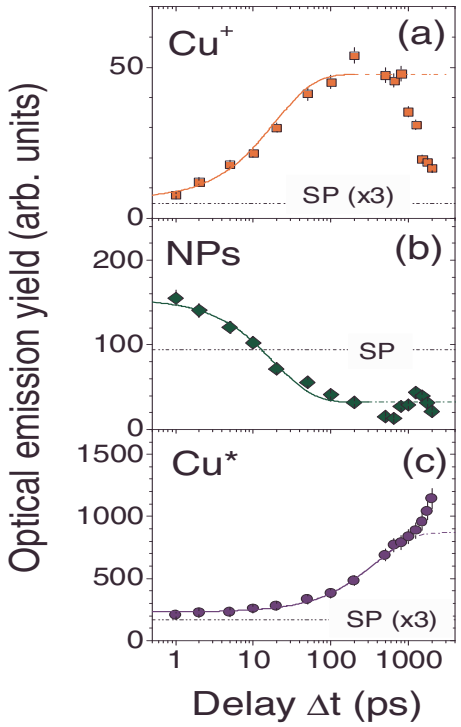

FIG. 10. (Color online) Optical emission yield of the various plume components as a function of the time delay Δt between the pulses: (a) Cu^+; (b) NPs; and (c) Cu^*. The dashed lines show the values corresponding to SP irradiation. The solid lines are fits to an exponential dependence of the emission intensity on Δt [see Eqs. (2) and (3)].

lines, as well as a faint Cu^+ emission at 505.18 nm; (ii) some characteristic, persistent emission lines at 510.55, 515.32, and 521.82 nm due to excited neutrals (Cu^*) contributing to the very intense core of the atomic plume emission of Fig. 7(a) and some other weaker Cu^* emission lines (e.g., 406.2 nm and 578.2 nm); (iii) the typical structureless, broadband emission of a slow population of NPs following the faster atomic plume (see the upper panel at $\Delta t=2$ ps, e.g.),[28] which are still very close to the target surface at 200 ns after the ablating laser pulse [see Fig. 7(a)].

The spectra of Fig. 8 shows a continuous increase in the Cu^* emission intensity with the delay Δt, while the variation in the Cu^+ emission signal is nonmonotonic, first rising up and reaching a maximum at $\Delta t \approx 100$ ps, and then declining at larger delays. Besides, the NP broadband emission significantly decreases with the delay Δt. This is still more evident in Fig. 9, where the 1D spectrally resolved images registered 2 μs after the ablating pulse are reported. Moreover, the regions of maximum emission of Cu^* and Cu^+ in Fig. 8 gradually move toward the target surface as Δt increases, the atomic emission lines approaching the NP region of emission close to the target surface ($z=0$) at the larger delays, as already observed before in the images of Fig. 7(a). In the spectra of Fig. 9, the presence of slower Cu^* atoms at increasing delays can also be ascertained, thus suggesting that a component of low-energy excited neutrals is formed in the atomic plume at longer delays, similarly to what has been already observed for the ions in Sec. III B.

A more quantitative characterization of the dependence of the three different plume components (Cu^+, Cu^*, and NPs) with the delay Δt between the pulses was obtained by recording the overall emission spectra of the atomic and NP plumes, and spatially and spectrally integrating the different contributions. The results are summarized in Fig. 10; the dashed-dotted line in each plot shows the value corresponding to the SP irradiation. The optical emission yield of Cu^+ obtained by integrating the signal at ≈490 nm and reported in Fig. 10(a) shows a behavior very consistent with that observed for the ions yield collected by the Langmuir probe in Fig. 4(b). The curve in Fig. 10(a) is a fit of the Cu^+ optical emission yield to Eq. (2) for 1 ps $<\Delta t<$ 200 ps ($Y_0 \approx 6.7$ and $\Delta Y \approx 41$) which yields the same characteristic time constant $\tau_c \approx 20$ ps already observed for the collected ion yield in the interval 1 ps $<\Delta t<$ 200 ps. Figure 10(b) reports the NPs emission yield versus Δt. The NP signal is significantly reduced for 1 ps $<\Delta t<$ 200 ps, following a trend which is well described by an exponential dependence similar to Eq. (1), i.e.,

$$Y_{NP}(\Delta t) = Y_{NP,0} - \Delta Y_{NP}(1 - e^{-\Delta t/\tau_c}), \quad (3)$$

with a characteristic time constant $\tau_c \approx 20$ ps [solid curve in Fig. 10(b)]. At larger delays ($\Delta t \geq 300$ ps) the data are somewhat scattered, but still remain at rather low values being approximately described by a plateau regime [dashed curve in Fig. 10(b)]. Interestingly, the same functional behavior of the ablation efficiency and NP optical yield suggests that decrease in the NP emission signal is mainly due to a reduced ablation efficiency of DP ULA, consistent with the observation that the ablated material of an ULA process mainly decomposes into a nanoparticulate form.[2,6,7,14] The reduction in the NP optical yield and ablation efficiency for 1 ps $<\Delta t<$ 200 ps is also very well correlated with the enhancement of the ion yield. This strict association can be

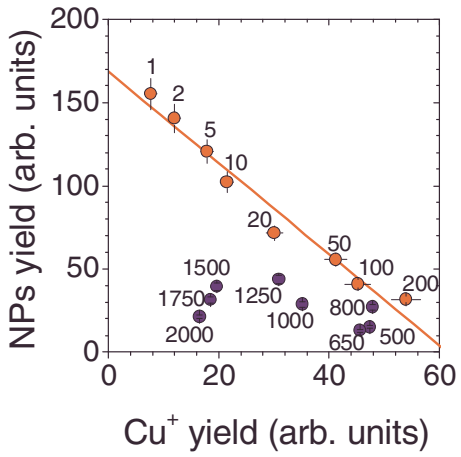

FIG. 11. (Color online) NP vs Cu^+ optical emission yields. The straight line is a linear fit showing a strict correlation between the two quantities for 1 ps $< \Delta t <$ 200 ps (the correlation coefficient is $r=-0.984$).

clearly appreciated by plotting the values of Cu^+ and NP optical emission yield against each other as in Fig. 11. The data are very well correlated in the range 1 ps $< \Delta t <$ 200 ps (the correlation coefficient is $r=-0.984$), thus suggesting that their opposite variation on Δt is due to the same underlying physical mechanisms. Instead, for $\Delta t \geq 300$ ps, the link between these two physical quantities is progressively reduced being finally lost as Δt increases further.

The optical emission yield of Cu^*, obtained by integrating the signals of the 510.55, 515.32, and 521.82 nm emission lines, is shown in Fig. 10(c). The atomic emission is also well described by an exponential dependence [Eq. (2)] for $\Delta t \leq 800$ ps but with a larger characteristic time constant $\tau_c \approx 400$ ps. This exponential trend is then followed by another regime characterized by a further increase in the emission signal. It is likely that this different behavior of the optical emission yield of the excited neutrals results from the generation of the low-energy component whose contribution was observed to progressively increase with the delay Δt. Therefore, the optimal conditions for the enhancement of excited neutrals seem to be rather different than those for the ions, in our experimental conditions.

IV. DISCUSSION

The experimental results illustrated in the previous section show the existence of different regimes of interaction in DP ULA of a metallic target resulting from the interplay between the different mechanisms involved in the process. Particularly, interesting is the correlation between the reduction in the ablation efficiency and NP plume emission intensity and the increase in the ion yield for delays $\Delta t \leq 100$ ps. Besides, at larger delay it is noticeable that both ablation efficiency and NP plume emission tends to a plateau while the optical emission from neutrals is further enhanced and the ions signal decreases. These experimental observations refer to a fluence per pulse of ≈ 4 times the ablation threshold, a regime of interest for a deeper understanding of the mechanisms involved in the DP ULA process, as well as for possible interesting outcomes in a class of ULA-based applications, e.g., femtosecond laser machining, LIBS, NP synthesis, plasma generation, and film growth through ultrafast pulsed laser deposition.

A reasonably clear picture of SP ULA of metals has now emerged thanks to an extensive experimental work,[7,10,11,15,16] and a number of theoretical analyses of the decomposition mechanisms.[5–9,12,13] However, DP ULA experiments and modeling are still rather limited. In DP ULA the effects brought about by the irradiation with a second pulse will depend critically on how the near-surface region of the target has evolved since the delivery of the first pulse and thus on the delay Δt between the pulses. In particular, for a delay Δt much less than the electron-lattice relaxation time τ_{el}, the DP irradiation is expected to be rather similar to one SP with the same overall fluence. On the other hand, for a delay larger than τ_{el} the second pulse can interact either with a modified target surface or with the complex, structured material progressively released from the target surface which finally gives rise to the two distinct ablation plumes observed in the far field: a faster-moving atomic plume and a slower-moving NPs plume.[15,28] For copper τ_{el} is of the order of 10 ps.[22]

Povarnitsyn *et al.*[22] have carried out hydrodynamic modeling of DP ULA of copper mainly highlighting the effect of the delay Δt between the pulses on the target decomposition mechanisms, which finally results in the decrease in the crater depth observed experimentally.[1,2,20] This study confirmed that when Δt is much shorter than τ_{el}, both pulses contribute to ablation, similar to the case of one pulse with twice the fluence. For Δt of the same order of τ_{el}, the second pulse interacts with the front of the nascent ablation plume reheating the ablated material and generating a high-pressure region in the vicinity of the decomposing target surface. This, in turn, produces a shock wave that reduces the intensity of the ablating rarefaction wave in the target, thus leading to a decrease in the ablation efficiency. Finally, for Δt much longer than τ_{el}, the ablation crater is mainly formed by the first pulse while the second pulse interacts with the ablating material without inducing any additional removal of material from the target. This description is consistent with the behavior of the ablation efficiency of Figs. 1 and 3. In particular, in Fig. 3 we observed a $\approx 30\%$ reduction in the ablation depth at $\Delta t \approx \tau_{el}$, and a plateau for $\Delta t > 100$ ps.

The experimental results of Secs. III B and III C reveal the changes induced in the ULA plumes by the interaction of the second pulse with the ablating material, at the different stages of the target decomposition and ablation process. Partial absorption of the second pulse in the front layer of the nascent ablation plume explains the observed increase in both the yield [Figs. 4 and 10(a)] and energy (Fig. 5) of the ions for $\Delta t \leq 100$ ps. This process seems to reach an optimal state at ≈ 50 ps, in our experimental conditions. The correlated reduction in the ablation efficiency and NP optical emission (see Figs. 3, 10, and 11) is also consistent with a decrease in the energy coupling to the target. In this respect, it is worth noting that in Ref. 22 an average absorption coefficient $A \approx 0.35$ for the second pulse was estimated at a delay of ≈ 50 ps. This absorption occurs in a front layer of the nascent ablation plume with a thickness $\Delta z \approx 200$ nm, which corresponds to an average linear absorption coefficient

$\alpha = -\Delta z^{-1} \times \ln(1-A) \approx 2 \times 10^4$ cm^{-1}. By taking into account that the average density n of the absorbing layer in Ref. 22 is $\approx$7%–8% of the solid density (for copper $n_s = 8.46 \times 10^{22}$ cm^{-3}), we can estimate an absorption cross section of the nascent ablation plume $\sigma_{abs}(=\alpha/n)$ of the order of few $\times 10^{-18}$ cm^2, at $\Delta t \approx 50$ ps.

In an attempt to clarify the optical properties of the front layer produced in the first stages of the ULA process, we have calculated the total absorption cross section of a high-density, high-temperature material whose properties resemble the nascent front layer produced during ULA of metals. Molecular dynamics simulations and hydrodynamic modeling of ULA of metals show that, at a delay of 20–100 ps after the ablation pulse, the front layer density n and temperature T are of the order of $(0.01-0.1) \times n_s$ and several thousand kelvin.[6,7,9,22,29] The total optical absorption cross section was obtained by using a spectral synthesis codes (e.g., PRISMSPECT) (Ref. 30) modeling plasma ionization, level populations, line broadening, and spectral emission and absorption for a plasma with temperature and density given above. The estimated absorption cross section σ_{abs} at 527 nm (2.35 eV) is always of the order of few $\times 10^{-18}$ cm^2 in the density range $10^{19}-10^{22}$ cm^{-3}, at a temperature of several thousand kelvin, in agreement with the prediction of Ref. 22. This indicates a total absorption cross section of the front of the ablation material which is only slightly reduced and of the same order of magnitude of that for solid copper at room temperature (7.8×10^{-18} cm^2). At an average fluence level of few times the ablation threshold, which corresponds to $\approx 10^{18}$ photons/cm^2, there is a significant probability ($\approx$0.8–1.0) that the atoms of the front layer absorb photons from the second pulse producing a temperature rise with a consequent increase in the ionized and excited species in the atomic plume, as experimentally observed.

To a first approximation it can be assumed that the observed increase in the ions and excited neutrals ΔY is proportional to the fraction of energy absorbed from the second pulse, E_{abs}

$$\Delta Y(\Delta t) \propto E_{abs} \propto 1 - \exp[-A^*(\Delta t)], \tag{4}$$

where $A^*(\Delta t)$ is the absorbance of the nascent plume at delay Δt. Therefore, the yield $Y(\Delta t)$ at delay Δt can be expressed as $Y(\Delta t) = Y_0 + \Delta Y(\Delta t)$, Y_0 corresponding to the yield at short delays ($\Delta t \ll \tau_{el}$). Since the energy diffusion length into the target is small and τ_{el} is short, to a first approximation the physical phenomenon occurring at the target surface is rather similar to the one occurring after an impulsive heating of a thin near-surface layer of a semi-infinite solid medium.[29,31] In this case, a compression or shock wave propagates into the bulk of material, while an unloading rarefaction wave forms leading to material release and expansion from the original target surface into vacuum. The front of the rarefaction wave expands with a characteristic velocity u_{exp} while the density profile $n(z, \Delta t)$ of the released material is characterized by an exponential profile[31,32]

$$n(z, \Delta t) = n_0 \exp\left(-\frac{z}{u_{exp}\Delta t}\right), \tag{5}$$

where n_0 is the density at the position $z=0$ of the original surface and is given by $n_0 = n_s/e$, where n_s is the atomic density of the target material and e is the Neper number. In this respect, it is worth observing that an approximately exponential density distribution of the atomic front layer of the ablation material produced during ULA was observed by ultrafast time-resolved x-ray absorption spectroscopy in Ref. 15, though the measurements reported in the paper refer to much longer delays ($\geq$500 ns). In ULA, as time Δt elapses after the laser pulse, the rarefaction wave continues to add material to the nascent plume. The average absorbance $A^*(\Delta t)$ is given by

$$A^*(\Delta t) = \int_0^\infty n(z, \Delta t)\sigma_{abs}(z, \Delta t)dz \approx n_0 \sigma_{abs} u_{exp} \Delta t, \tag{6}$$

where an average value σ_{abs} has been considered due to the slowly varying dependence of the absorption cross section on the layer physical properties. By using Eqs. (6) and (4) the observed exponential dependence of Eq. (2), which fits fairly well the experimental data of Figs. 4(b) and 10(a), is finally obtained. An estimate of the characteristic time constant τ of such dependence can be obtained by considering $A^*(\tau) \approx 1$, which yields $\tau \approx (n_0 \sigma_{abs} u_{exp})^{-1}$. Both experimental characterization[15] and modeling[29] of the initial stages of ULA of a metallic target show an expansion velocity of the nascent ablation plume of the order of $u_{exp} \approx 10^5-10^6$ cm/s, while the velocity of the density maximum can be about ten times less. Therefore, for $n_0 \approx$ few $\times 10^{22}$ and $\sigma_{abs} \approx$ few $\times 10^{-18}$ cm^2, values of the characteristic time constant τ of the order of $\approx$10–100 ps are fully justified and indeed experimentally observed by us and others.[2,23] The fact that Eq. (2) describes rather well the experimental data for $\Delta t \leq 100$ ps also indicates that the properties of the front of the nascent ablation plume vary slowly in this regime, probably as a consequence of the continuous supply of material from the target over this time interval.

In the regime where the second laser pulse is efficiently absorbed ($\Delta t \leq 100$ ps), the ablation efficiency falls significantly (see Fig. 3), as a consequence of both a reduced energy transfer into the target and of the effects brought about by the pressure wave induced by the interaction of the second laser pulse with the expanding material, as discussed in Ref. 22. Since in ULA the deeper layers of the original target mainly decompose in the form of nanoaggregates, the reduced ablation efficiency is also manifested by a reduction in the NP emission signal intensity [Fig. 10(b)]. Moreover, the absorption of the second laser pulse also causes the observed increase in ionization, which explains the strict correlation observed in this regime between the NP plume emission intensity and the ion yield (Fig. 11). By considering that the contribution of the second pulse to the ablation efficiency is proportional to the fraction of its energy reaching the target one can derive the dependence reported in Eq. (1), which fits rather well the experimental data of Fig. 3. In this respect, it

is also worth noting that Eq. (1) also describes fairly well the theoretical predictions of the ablation depth reported in Ref. 22.

As the delay Δt increases beyond a value around 100 ps, both the density and temperature of the absorbing front layer progressively decreases and its absorption cross section at the laser wavelength drops down. Moreover, in some cases hydrodynamic modeling also predicts a separation of the front layer from the rest of ablating material after a certain delay, indicating the end of the material supplied to this front component of the ablation plume. Therefore, the atomic front layer becomes gradually more transparent to the second laser pulse, which explains the reduction in the ions yield at larger delays observed in Figs. 4(a) and 10(a). Consequently, an increasingly larger fraction of the second pulse reaches the inner regions of the ablating material. Since the deeper regions decompose in the form of a hot-liquid-phase material which relaxes into a nascent NP plume expanding at lower velocity,[7,22,29] this interaction eventually produces further atomization and ionization through NP break-up processes, thus leading to the occurrence of an atomic emission increasing over a longer time interval with respect to ions, as observed in Fig. 10. At very long delays ($\Delta t > 500$ ps), the additional increase in this emission evidences a still more efficient coupling of the second pulse with the inner regions of the ablating material. It seems also that in our experimental conditions this interaction does not produce a simultaneous increase in ionized species. This can be understood if one compares this situation to SP ULA in the same experimental conditions,[23] where only an extremely faint ion emission signal is observed at the same fluence level. A similar behavior of the ions and excited neutrals emission was instead observed at comparable delays for Ti in Ref. 4 and for Cu in Ref. 33. This seems to suggest a rather significant influence of the specific experimental conditions (e.g., laser pulse fluence, wavelength, and target physical properties) on the interaction between the second pulse and the nascent ablation material, where the coupling of the second laser pulse to the hot-liquid-phase material ejected later in time can be strongly mediated by the specific properties of the nascent ablation plume. This is indeed supported by the reduction in the DP delay needed to approach the SP ablation depth at larger fluences experimentally observed in DP ULA of silver targets.[21]

Finally, in this regime ($200 \leq \Delta t \leq 2$ ns) both the ablation efficiency (Fig. 2) and NP emission [Fig. 10(b)] remain low, indicating that the second pulse does not cause any additional emission of material from the target. This is probably due to the interaction of the second pulse with the decomposing hot-liquid-phase material which hinders efficient transport of energy to the rest of the target. Efficient coupling of the second laser pulse energy to the target is predicted to occur only after delays of the order of tens of nanoseconds or more,[22] when the material ablated by the first pulse becomes completely transparent, a timescale which has not yet been achieved in DP experiments.

V. CONCLUSION

In this investigation, experiments aiming to explore various aspects of DP ULA of a metallic target were carried out with the aim of addressing the changes to the ablation efficiency and to the properties of the ablation plumes as a function of the delay Δt between the pulses. Our experimental results confirm the reduction in the ablation efficiency with the delay Δt reported earlier by us and others,[1,2,20,21] interpreted in terms of the interaction of the second pulse with the front of the nascent ablation plume reheating the ablated material and to the effects brought about by such interaction. The analysis of the ablated species allowed us to identify the other effects of this interaction and the characteristic timescale of the induced changes. In particular, an interesting increase in the ion yield was observed for $\Delta t \leq 100$ ps, which is well correlated with the reduction in the NP yield and ablation depth.

A simple model based on impulsive heating of a thin near-surface layer of a semi-infinite solid medium and on the exponential density profile of the released material corroborates the experimentally observed dependencies, also providing estimate of the characteristic time constant in fairly good agreement with the experimental findings. The good consistency of the model predictions and experimental observations suggests that this relatively simple model describes the main features of DP ULA of metallic targets.

We consider that several of the features observed in the present investigation on a copper target can be considered as rather general aspects of the DP ULA of metals at moderate laser intensities. The experimental results obtained and interpretation will be particularly helpful in the design of strategies to improve the control and/or manipulate the characteristics of the plumes of material generated in ULA processes. This, in turn, is important for the various applications of ULA in fields like material deposition and film growth, NP generation, material microprobe analysis with LIBS, laser produced plasmas, and so forth.

ACKNOWLEDGEMEMTS

We acknowledge financial support from Science Foundation Ireland under Grant No. 09/RFP/PHY2422.

[1] T. Donnelly, J. G. Lunney, S. Amoruso, R. Bruzzese, X. Wang, and X. Ni, J. Appl. Phys. **106**, 013304 (2009).
[2] S. Noël and J. Hermann, Appl. Phys. Lett. **94**, 053120 (2009).
[3] R. Stoian, A. Mermillod-Blondin, N. M. Bulgakova, A. Rosenfeld, I. V. Hertel, M. Spyridaki, E. Koudoumas, P. Tzanetakis, and C. Fotakis, Appl. Phys. Lett. **87**, 124105 (2005).
[4] D. Scuderi, O. Albert, D. Moreau, P. P. Pronko, and J. Etchepare, Appl. Phys. Lett. **86**, 071502 (2005).
[5] M. Spyridaki, E. Koudoumas, P. Tzanetakis, C. Fotakis, R. Stoian, A. Rosenfeld, and I. V. Hertel, Appl. Phys. Lett. **83**, 1474 (2003).
[6] M. E. Povarnitsyn, T. E. Itina, M. Sentis, K. V. Khishchenko, and P. R. Levashov, Phys. Rev. B **75**, 235414 (2007).
[7] S. Amoruso, R. Bruzzese, X. Wang, N. N. Nedialkov, and P. A. Atanasov, J. Phys. D: Appl. Phys. **40**, 331 (2007).
[8] P. Lorazo, L. J. Lewis, and M. Meunier, Phys. Rev. B **73**, 134108 (2006).
[9] C. Cheng and X. Xu, Phys. Rev. B **72**, 165415 (2005).
[10] S. Amoruso, R. Bruzzese, N. Spinelli, R. Velotta, M. Vitiello, X. Wang, G. Ausanio, V. Iannotti, and L. Lanotte, Appl. Phys. Lett. **84**, 4502 (2004).
[11] S. Eliezer, N. Eliaz, E. Grossman, D. Fisher, I. Gouzman, Z. Henis, S. Pecker, Y. Horovitz, M. Fraenkel, S. Maman, and Y. Lereah, Phys. Rev. B

69, 144119 (2004).
[12]D. Perez and L. J. Lewis, Phys. Rev. B **67**, 184102 (2003).
[13]D. Bouilly, D. Perez, and L. Lewis, Phys. Rev. B **76**, 184119 (2007).
[14]S. Amoruso, R. Bruzzese, X. Wang, and J. Xia, Appl. Phys. Lett. **92**, 041503 (2008).
[15]K. Oguri, Y. Okano, T. Nishikawa, and H. Nakano, Phys. Rev. B **79**, 144106 (2009).
[16]S. Amoruso, R. Bruzzese, M. Vitiello, N. N. Nedialkov, and P. A. Atanasov, J. Appl. Phys. **98**, 044907 (2005).
[17]R. Hergenröder, M. Miclea, and V. Hommes, Nanotechnology **17**, 4065 (2006).
[18]M. Guillermin, C. Liebig, F. Garriele, R. Stoian, A.-S. Loir, and E. Audouard, Appl. Surf. Sci. **255**, 5163 (2009).
[19]V. Piñon, C. Fotakis, G. Nicolas, and D. Anglos, Spectrochim. Acta, Part B **63**, 1006 (2008).
[20]A. Semerok and C. Doutouquet, Thin Solid Films **453–454**, 501 (2004).
[21]D. E. Roberts, A. du Plessis, and L. R. Botha, Appl. Surf. Sci. **256**, 1784 (2010).
[22]M. E. Povarnitsyn, T. E. Itina, K. V. Khishchenko, and P. R. Levashov, Phys. Rev. Lett. **103**, 195002 (2009).
[23]S. Amoruso, R. Bruzzese, and X. Wang, Appl. Phys. Lett. **95**, 251501 (2009).
[24]M. Liu, Opt. Lett. **7**, 196 (1982).
[25]B. Doggett and J. G. Lunney, J. Appl. Phys. **105**, 033306 (2009).
[26]J. Bonse, H. Sturm, D. Schmidt, and W. Kautek, Appl. Phys. A: Mater. Sci. Process. **71**, 657 (2000).
[27]W. C. Martin, J. R. Fuhr, D. E. Kelleher, A. Musgrove, J. Sugar, W. L. Wiese, P. J. Mohr, and K. Olsen, *NIST Atomic Spectra Database (Version 2.0)* (National Institute of Standards and Technology, Gaithersburg, MD, 1999); Available online at: http://physics.nist.gov/asd
[28]S. Amoruso, G. Ausanio, R. Bruzzese, M. Vitiello, and X. Wang, Phys. Rev. B **71**, 033406 (2005).
[29]T. E. Itina, J. Hermann, Ph. Delaporte, and M. Sentis, Thin Solid Films **453–454**, 513 (2004).
[30]http://www.prism-cs.com/Software/PrismSpect/PrismSPECT.htm
[31]Y. B. Zel'dovich and Y. P. Raizer, *Physics of Shock Waves and High-Temperature Hydrodynamic Phenomena* (Academic, London, 1966).
[32]D. Attwood, *Soft X-Ray and Extreme Ultraviolet Radiation, Principles and Applications* (Cambridge University Press, Cambridge, 1999).
[33]X. Wang, S. Amoruso, and J. Xia, Appl. Surf. Sci. **255**, 5211 (2009).